# Oligocene - early Miocene river incision near the first bend of the Yangze River: Insights from apatite (U-Th-Sm)/He thermochronology

Xiaoming Shen [a], Yuntao Tian [b], Dewen Li [a], Siwei Qin [a], Pieter Vermeesch [b], James Schwanethal [b]

a *Key Laboratory of Crustal Dynamics, Institute of Crustal Dynamics, CEA, Beijing 100085, China*

b *Department of Earth Sciences, University College London, London WC1E 6BT, UK*

Corresponding author:
Yuntao Tian
Department of Earth Sciences
University College London
Gower Street
London, WC1E 6BT
United Kingdom
Email: y.t.tian@ucl.ac.uk

**Abstract**

The southeastern Tibetan Plateau is deeply incised by three parallel rivers, the Salween, the Mekong and the Yangtze. The river incision and surface uplift histories of this landscape are hotly debated. This study presents bedrock apatite (U-Th-Sm)/He data from a ~1800m vertical profile, located near the first bend of the Yangtze River. Ages range from 20 to 30 Ma, indicating an Oligocene - early Miocene phase of moderate river incision at a rate of ~0.10-0.18 mm/yr. This is considerably older than elsewhere in the region, but consistent with a previously proposed phase of Eocene surface uplift inferred from stable isotope geochemistry. We consider the implications of the new data under two different tectonic models. If the surface uplift and river incision resulted from lower crustal flow, the new results require such flow to have commenced at Oligocene - Early Miocene time rather than during the previously proposed Late Miocene. Alternatively, Oligocene to Early Miocene plateau growth might have resulted from transpressional deformation in the southeastern Tibetan Plateau.

**Highlights:**

Oligocene - early Miocene river incision

Diachronous onset of river incision in the southeastern Tibetan Plateau

Oligocene to Early Miocene lower crustal flow or transpressional deformation

**Keywords:** River incision, Thermochronology, Tibetan Plateau, Yangtze River, (U-Th-Sm)/He, Landscape evolution

## 1. Introduction

It has been proposed that the formation of the Tibetan Plateau, which includes >80% of the world's land with elevation >4 km above sea level (e.g., Fielding et al., 1994), resulted from a series of continental accretions and collisions during Mesozoic and Cenozoic time (e.g., Powell and Conaghan, 1973; Patriat and Achache, 1984; Chang et al., 1986; Yin and Harrison, 2000). Development of the Tibetan Plateau is thought to have strongly influenced regional and even global geodynamics, as well as climate systems (e.g., Molnar and Tapponnier, 1975; An et al., 2001; Tapponnier et al., 2001). One of the most remarkable physiographic features of the Tibetan Plateau, revealed by high-resolution digital topographic data, is the presence of highly-incised river gorges in the plateau surrounding margins (Liu-Zeng et al., 2008). This is especially phenomenal in the three-rivers region in the southeastern part of the Plateau, where three parallel rivers, the Yangtze, Mekong and Salween, carve gorges up to 3 km deep (Fig. 1).

Various geodynamic models have been proposed to explain the formation of these river gorges. One school of thought is that the surface uplift of the region, as well as other plateau margins was formed by vertical thickening and lateral flow of the lower crust (e.g., Clark et al., 2005a; Schoenbohm et al., 2006). However, other models have highlighted the importance of crustal thickening, lateral extrusion, and rotation (e.g., Tapponnier et al., 2001), or crustal detachment fault (Tian et al. 2013, 2015). A recent computational study reproduced the topography of the southeast Tibetan Plateau under conditions of widespread crustal shortening and river network reorganization (Yang et al., 2015).

Debate continues as to the initiation time of the high-relief and high-elevation landscapes in the southeast Tibetan Plateau. Using river incision history, constrained by thermochronological data, as an index for relief-formation, it has been suggested that the southeastern Tibetan Plateau was formed during the late Miocene (9-12 Ma) (e.g. Clark et al., 2005b; Ouimet et al., 2010), the mid Miocene (15-22 Ma) (Tian et al., 2014), or even earlier at the southern Longmen Shan (Wang et al., 2012). A recent study by Yang et al. (2016) reconstructed the post 10Ma erosional pattern in the southeastern Tibetan Plateau. Worth noting is that this study reported several Oligocene thermochronological data from the sites along the Yangtze River. Further, a recent river incision study using cosmogenic dating of cave sediments at the first bend of the Yangtze River, where water-flow direction changes abruptly from southeast-ward to northeast-ward within a distance of 1 km, suggests a scenario in which ~1 km incision occurred between 18 and 9 Ma and ceased thereafter (McPhillips et al., 2016). Finally, palaeo-altimetry studies using stable isotopes suggest that the southeastern Tibetan Plateau might have gained a high elevation of ~3 km at Eocene time (Hoke et al., 2014; Li et al., 2015).

The river incision and surface uplift histories of the area near the first bend of the Yangtze River have been addressed by several recent studies using multiple methods, including cosmogenic nuclides of cave sediments (McPhillips et al., 2016), palaeo-altimetry (Hoke et al., 2014; Li et al., 2015), and morphometric indices (Liu-Zeng et al., 2008), as introduced above. This makes the area an ideal place for testing the consistency of different methods. However, thermochronometric data, which are sensitive to near-surface deformational and erosional processes (e.g., Gleadow et al., 2002; Farley, 2002), remain unavailable in the area. The present study applies apatite (U-Th)/He (AHe) dating to a group of bedrock samples from the Laojunshan felsic intrusions, ~25 km southwest of the first bend (Figs. 1, 2). Results suggest a significant phase of river incision at 30-20 Ma. In the context of previous river incision studies, our results indicate that crustal thickening, surface uplift and river incision in the field area may have initiated in pre-Miocene time, rather than during the late Miocene, as was suggested by previous thermochronometric studies elsewhere in the region.

## 2. Topographic and geological background

The study area is located near the first bend of the Yangtze River in the southeast Tibetan Plateau (Fig. 1, 2). Peak elevations of the area exceed 4200 m, whereas river valleys have incised down to elevations of <2000 m, forming a regional topographic relief of more than 2200 m (Fig. 2).

From a tectonic perspective, the study area lies on the western margin of the South China Block, with the Lhasa and Qiangtang Blocks to the west, the Songpan-Ganze Block to the north, and Indochina block to the south (Fig. 1a). These blocks were separated by large-scale strike-slip faults such as the Jinsha-Red River fault, which play an important role in the accommodation of crustal deformation during plateau formation (Tapponnier et al., 2001; Shen et al., 2005).

Surface outcrops in the area mainly consist of Paleozoic to Mesozoic sandstone, limestone, metamorphic and volcanic rocks, and Cenozoic high-K volcanics, volcanic breccia, and terrestrial deposits, including conglomerate, sandstone, siltstone, and mudstone (YBGMR, 1984). Eocene felsic intrusions, which are collectively referred as the 'Laojunshan intrusion', mainly consist of syenite or orthophyre, granite, and quartz monzonite (Fig. 2) (Lu et al., 2012). Zircon U-Pb dating of these intrusive rocks suggests that they were formed at ~35-36 Ma (Schärer et al., 1994; Lu et al., 2012; Wan et al., 2006). It has been proposed that these intrusive rocks were associated with late Eocene continental subduction or delamination of overthickened lithospheric mantle following the collision between India and Asian (Wang et al., 2001; Chung et al., 2005; Lu et al., 2015).

All the samples analysed in this study were collected from the Laojunshan intrusion (Fig. 2), which intrudes a succession of Cenozoic sediments in the Jianchuan basin comprised of the following formations. The Yunlong formation unconformably overlies Mesozoic strata consists of purple–red, fine-grained siltstones and mudstones with several gypsum horizons (YBGMR, 1974). The formation is overlain by a volcanic horizon, whose 36-35 Ma age has been constrained by zircon U/Pb dating (Yang et al., 2014). Overlying the Eocene strata, are several poorly dated formations consisting of siltstone, sandstone, conglomerate and coal layers. On the basis of fossil plants data, Zhao et al. (1965) suggested those rocks are of Miocene-Quaternary time, and that Oligocene strata are regionally missing in the basin. However, a recent study of Gourbet et al. (2015) suggested nearly no post 34 Ma sedimentation.

## 3. Methodology and results

### 3.1. Sampling strategy

Low temperature thermochronological (notably apatite fission track [AFT] and apatite (U-Th-Sm)/He [AHe]) data from vertical profiles can provide constraints on the erosional history of tectonically active terranes (e.g., Fitzgerald et al., 1986), as discrete phases of rapid river incision result in positive age-elevation relationships. In this study, seven intrusive rock samples were collected from several Eocene felsic intrusions around the Laojunshan Mountains. Samples' elevations range from the peak of the Laojunshan (4247 m) to the deeply incised valley of a tributary of the Yangtze River (2162 m), forming a vertical profile spanning ~ 1800 m relief over a lateral extent of ~ 20 km (Fig. 3). It is worth noting that the intrusion, from which the samples were collected, is an undeformed Eocene pluton, in which no faulting has been observed during field investigations.

### 3.2. Experimental methodology

Apatite concentrates were produced using standard crushing, sieving, electromagnetic, and heavy liquid mineral separation techniques. Inspection of polished and etched mineral separates revealed the common occurrence of crystal dislocations (see appendix A1) which impede the confident identification and counting of fission tracks. Thus only AHe data are presented in this study.

To this end, apatite grains were picked and examined at ×250 magnification to detect possible mineral inclusions. Only clear and euhedral grains were selected for AHe analysis.

Protocols for AHe analysis followed an established laboratory routine for laser He extraction (House et al., 2000). Samples were loaded into platinum capsules and outgassed under vacuum at ~900 ˚C for 5 minutes using a fibre-optically coupled diode laser with a 808 nm wavelength, then spiked with $^{3}$He and gas volumes determined using a Pfeiffer plasma quadrupole mass analyser. Molar abundances of U and Th were determined by isotope dilution using a mixed $^{235}$U-$^{230}$Th spike. The Sm abundance was determined by comparison with a standard solution of known U/Sm ratio. U-Th-Sm analyses were carried out by ICP-MS, using an Agilent 7700x quadrupole mass spectrometer. Apparent AHe ages were calculated and corrected for α-emission following the approach of Ketcham et al. (2011). Reported uncertainties of the AHe data are ~5% (1σ), which includes a 5 μm uncertainty in grain size measurements for the α -ejection correction. Durango apatite was run as an external standard with each batch of samples as an additional check of the analytical accuracy.

**3.2. Results and interpretation**

Four single-grain AHe age analyses were performed for each of the seven Laojunshan samples. The samples yield mostly consistent AHe ages, although anomalously old grains are not uncommon, as described next. The lowest elevation sample SG1402 (2162 m), yielded three concordant single-grain AHe ages of 21-25 Ma and one 40.1 ± 2.0 Ma age, which is older than the crystallization age of Laojunshan intrusion (35-36 Ma, Lu et al., 2012) (Fig. 3). Moving up the vertical section, samples SG1407 (2326 m) and LJS1401 (2942 m) yield single-grain AHe ages ranging from 12.7 ± 0.6 Ma to 21.9 ± 1.1 Ma, and from 19.9 ± 1.0 Ma to 30.7 ± 1.5 Ma, respectively. These ages do not show clear relationships with the effective Uranium ([eU] = [U] + 0.235 × [Th]) contents (Fig. 4a), nor with the grain size (Fig. 4b). Three of the four single-grain ages of sample LJS1403 (3300 m) fall in a range of 40-50 Ma, which again is older than the crystallization age of Laojunshan intrusion, with the remaining grains being slightly younger at 31.4 ± 1.6 Ma. These grains have relatively low [eU] contents (9-12 ppm), and relatively large grain sizes (110-210 μm). Sample LJS1404 (3611 m) yielded four single-grain ages between 17-33 Ma. Sample LJS1410 (3849 m) has four reproducible ages between 25 ± 1.3 Ma and 27.3 ± 1.4 Ma. The four single-grain ages of sample LJS1414 (3984 m) include two young ages of 27.2 ± 1.4 Ma and 29.2 ± 1.5 Ma, and two abnormally old ages of 45.3 ± 2.3 Ma and 57.9 ± 2.9 Ma, which are older than the intrusion age.

In summary, the AHe results include six grains that yield age that are older than the 35-36 Ma intrusion age, and are difficult to explain even though the grains exhibit a range of

[eU] contents (10-100 ppm) and grain sizes (50-200 μm) (Fig. 4 and Table 2). Although a progress has been made in explaining overdispersed and anomalously old (U-Th)/He ages (Fitzgerald et al., 2006; Flowers et al., 2009), no universal mechanism has been found to explain why some samples yield consistent (U-Th)/He data and others do not. For example, U-zoning in the core leads to overestimate of the alpha-ejection correction, but cannot explain the abnormally old ages in our study, because even the uncorrected ages of five of the six grains are older than the intrusion age (~35-36 Ma). Additional sources of $^{4}$He other than the analysed apatite, such as U-rich mineral inclusions in apatite, U-rich neighbouring minerals (Spiegel et al., 2009) may be possible explanations for those outliners.

Excluding the six abnormally old ages, the remaining 22 ages show a positive relationship with the elevations (Fig. 5b). Most of these ages cluster between 20-30 Ma (Fig. 5), even though they cover an 1800 m elevation range. These results have two important implications. (1) The age-elevation relationship suggests that the study area has experienced a phase of Oligocene – early Miocene moderate river incision at a rate of ~0.10-0.18 mm/yr, resulting from headward propagation of river incision from the trunk stream of the Yangtze River. (2) Post ~20 Ma, the samples remained at sub-80 °C temperatures. Assuming a geothermal gradient of 30-35 °C/km, this implies that post-mid Miocene exhumation was limited to less than ~2.5 km.

## 4. Discussion

### 4.1. River incision and surface uplift

Both the timing and magnitude of river incision in the study area differ from those in other sectors of the southern Tibetan Plateau. Besides the Laojunshan area, Oligocene to Early Miocene phase of river incision has only been identified in the Longmen Shan (Wang et al., 2012; Guenthner et al., 2014). In other adjacent areas, previous low-temperature thermochronological studies suggest that river incision occurred later in the Miocene (Kirby et al., 2002; Clark et al., 2005b; Enkelmann et al., 2006; Godard et al., 2009; Ouimet et al., 2010; Tian et al., 2013, 2015). Further, the amount of post ~20 Ma cooling (< 80 °C) and erosion (< 2.5 km) in the study area is significantly lower than in other areas, where those previous studies suggested an average post ~12 Ma erosion rate of 0.3-1.0 mm/yr. The lateral variation in erosion observed in this work is also supported by the Oligocene AHe ages from the downstream sites, as reported in Yang et al. (2016).

Assuming that surface uplift is coupled with river incision, the history of river incision and associated crustal cooling, as constrained by the means of low-temperature thermochronology, can be used to estimate the history of surface uplift (e.g., England and Molnar, 1990). Based on this assumption, our results indicate that the onset of the surface uplift at the Laojunshan site near the First Bend occurred before or during the Oligocene to Early Miocene (~30-20 Ma). This interpretation is consistent with palaeo-elevation estimates based on the stable isotope composition of carbonates from nearby sedimentary basins, which indicates that the southeastern Tibetan Plateau has been near its present elevation since the late Eocene (Hoke et al., 2014; Li et al., 2015). However, it is also possible that a considerable lag between surface uplift and incision might exist in the study area. We cannot test this hypothesis, because our data can only provide a minimum constraint on the onset time of river incision.

Previous studies suggest that the late Miocene phase of river incision and surface uplift is uniform across wide areas of the southeastern Tibetan Plateau (Clark et al., 2005b; Ouimet et al., 2010; Tian et al., 2015). The Oligocene to Early Miocene erosion and surface uplift in the Laojunshan area is clearly inconsistent with those previous results. This has the following two alternative implications. Either (1) the Oligocene - Early Miocene erosion resulted from local glaciations, magma cooling, or local faulting, or (2) in other regions, late Miocene cooling and erosion may have reset and removed evidence for the earlier event, which may have affected the entire region. These two scenarios are further discussed below.

**4.2. Local glaciations, magma cooling, or faulting?**

Glaciation in the southeastern Tibetan Plateau dates back to the Pleistocene (e.g., Yang et al., 2006; Owen, 2010; Fu et al., 2013). Any effects of Oligocene and Miocene glacial erosion would have been considerably weaker than today, because global mean temperature was considerably warmer back then (e.g. Zachos et al., 2008). Further, the present geometry of the gorge valleys near the First Bend is V-shaped, rather than U-shaped as is typical for glacial valleys.

The modeling of magma cooling suggests that the thermal anomaly associated with an igneous intrusion of ~10-km-radius would disappear in a short period (<1 Ma) (e.g., Ehlers, 2005). The observed cooling event at 30-20 Ma is more than 6 Ma later than the emplacement time of the intrusion (~35-36 Ma), and thus cannot be explained by simple post-emplacement cooling.

As for the faulting, the intrusions in the Laojunshan area are intact, and the sample locations are far away from nearby major faults (Fig. 2). The Weixi-Qiaohou and Longpan-Qiaohou faults which bound the study area have been identified as strike-slip faults since the Paleocene, as a westward extension of the Red River fault (e.g. Liu et al., 2004). No major differential rock uplift has been observed across these faults.

### 4.3. Oligocene to Early Miocene tectonics

Several lines of evidence suggest that the southeastern Tibetan Plateau may have experienced an Oligocene to Early Miocene (~30-20 Ma) phase of tectonic uplift. First, the Oligocene to Early Miocene erosion of the area is consistent with the Oligocene depositional hiatus in Jianchuan Basin surrounding the study area (Zhao et al., 1965; Gourbet et al., 2015). Second, the stable isotope data suggest that the elevation of the region around the First Bend has reached its present position at ~35 Ma (Hoke et al., 2014; Li et al., 2015), which is consistent with our results. Third, at the Daocheng River (an upstream tributary of the Yangze River), ~350 km inland, rapid river incision initiated at the Early Miocene (~22-15 Ma) (Fig. 1) (Tian et al., 2014). Combining the latter study with our new results implies that river erosion took 5-10 Myr to propagate headward from the study area to the Daocheng site. Fourth, in the central Longmen Shan, recent studies by Wang et al. (2012) and Guenthner et al. (2014) suggest a phase of rapid cooling during 30–20 Ma. Finally, the Oligocene to Early Miocene onset of river incision is also consistent with the sedimentation record in the South China Sea, whose sediments were fed by erosion of the southeastern Tibetan Plateau with the sedimentation rate peaking in the latest Oligocene to mid-Miocene (24–11 Ma) (Clift, 2006), suggesting that surface uplift in the southeastern Tibetan Plateau started during the Oligocene. Therefore, it is very likely that the Oligocene to Early Miocene river incision was a regional event, and a response to the eastward growth of the Tibetan Plateau.

Below we provide two possible tectonic models to explain the Oligocene – early Miocene growth of the southeastern Tibetan Plateau. First, we consider the implications of our data for the lower crustal thickening and flow model of Clark et al., (2005a) and Schoenbohm et al.(2006). Under this model, the Oligocene - Early Miocene phase of plateau growth observed in the present study would require such thickening and flow to have commenced at Oligocene - Early Miocene time rather than Late Miocene time (Clark et al., 2005b). According to the thermal-mechanical model of Beaumont et al. (2004), thickened crust may produce ductile flows that propagate into adjacent crust after a ~10-20 Myr period of lower crustal thermal weakening. This implies that the Tibetan hinterland may have acquired a thickened crust by ～50-40 Ma to produce the required Oligocene – early Miocene flow in the study area. Recent palaeoaltimetry results from the Linzizong Group in southern Tibet imply that the central Lhasa Block have achieved high elevations (~4.5 km), indicative of a thickened crust, at least by ～53 Ma (e.g., Ding et al., 2014). It is therefore possible to have a thickened and weak lower crust in the central Tibetan Plateau during the Oligocene, part of which flowed eastward to initiate the uplift of the southeastern Tibetan Plateau in Oligocene - Early Miocene time.

Alternatively, the Oligocene to Early Miocene onset of plateau uplift might indicate a different geodynamic process instead of lower crustal thickening and flow. In the crustal shortening and extrusion model (e.g., Tapponnier et al., 2001; Wang et al., 2001; Tian et al. 2014), the study area experienced a transpressional regime during Oligocene to Early Miocene time, characterised by north-south compression in the west and northwest-southeast left-lateral shearing in the east. This transpressional deformation would have resulted in regional surface uplift and extensive exhumation focused on the southeastern Tibetan Plateau (Tian et al., 2014).

This model is consistent with several geological records of the transpressional deformation in the southeastern Tibetan Plateau, as summarized next. (1) Cooling ages from the shear zones indicate that shearing along the Gaoligongshan-Chongshan and Ailaoshan shear zones occurred at 34-32 Ma (Wang et al., 2006; Akciz et al., 2008) and ~35 Ma (Leloup et al., 2001), respectively. (2) A belt of transpressional and transtensional basins formed during the Eocene to Neogene (SBGMR, 1991; Spurlin et al., 2005). These basins were rearranged by extrusion of the Indochina Block (Wang and Burchfiel, 1998), as evidenced by palaeomagnetic studies indicating that NW Yunnan has undergone ~90-45° of clockwise rotation (relative to the South China Block) since the Oligocene (Sato et al., 2007). (3) Recent studies reported several late Oligocene - early Miocene transpressional structures in the southeastern Tibetan Plateau (Tapponnier et al., 2001; Wang et al., 2012). (4) An Eocene to Oligocene (~40-30 Ma) potassic magmatic suite, whose geochemical signatures suggest coeval northeastward continental subduction or delamination of overthickened continental lithospheric mantle following the India-Asian collision, extends over 2000 km along a belt running from the central Tibetan Plateau to the southeastern Asia, via the study area (Wang et al., 2001; Chung et al., 2005; Spurlin et al., 2005; Lu et al., 2012). (5) To the west of the study area, early Miocene and earlier crustal compression occurred, as documented in the Hoh Xil and Yushu-Nangqian basins. In the Hoh Xil basin, studies of the strata, deformation, igneous activity, and exhumation of the basin have identified a phase of north-south shortening, which finished by ~30–22 Ma (Liu et al., 2001; Wang et al., 2008). (6) Detrital geochronology indicates that the present Yangtze River system was established after latest Oligocene drainage adjustment (Clift et al., 2006), which is considered to be synchronous with the start of strike-slip tectonism and surface uplift in southeastern Tibetan Plateau

(Zheng et al., 2013).

## 5. Conclusion

This work reports new AHe ages from the Laojunshan intrusion, near the first bend of the Yangtze River in the southeastern Tibetan Plateau. The ages cluster at 20-30 Ma, and show a positive relationship with elevation, suggesting a phase of Oligocene – early Miocene phase of moderate river incision at a rate of ~0.10-0.18 mm/yr.

These results are consistent with recent palaeoelevation reconstructions using the stable isotope composition of carbonates from the nearby sedimentary basins, which indicate that the southeastern Tibetan Plateau has been near its present elevation in late Eocene time. The newly identified Oligocene – early Miocene phase of river incision and surface uplift has the following two major implications. (1) It would require that lower crustal thickening and flow underneath the southeastern Tibetan Plateau to have commenced at Oligocene - Early Miocene time rather than the Late Miocene time suggested by previous studies. (2) Alternatively, Oligocene to Early Miocene plateau growth might have resulted from transpressional deformation in the southeastern Tibetan Plateau.

## Acknowledgements

This research was funded by NERC grant (#NE/K003232/1), National Natural Science Foundation of China (41203044) and the Basic Research Business Foundation of China Earthquake Administration (ZDJ2012-02).

## References

Akciz, S., Burchfiel, B.C., Crowley, J.L., Yin, J.Y., Chen, L.Z., 2008. Geometry, kinematics, and regional significance of the Chong Shan shear zone, Eastern Himalayan Syntaxis, Yunnan, China. Geosphere 4, 292-314.

An, Z.S., Kutzbach, J.E., Prell, W.L., Porter, S.C., 2001. Evolution of Asian monsoons and phased uplift of the Himalaya-Tibetan plateau since Late Miocene times. Nature 411, 62-66.

Beaumont, C., Jamieson, R.A., Mai, H.N., Medvedev, S., 2004. Crustal channel flows: 1. Numerical models with applications to the tectonics of the Himalayan-Tibetan orogen. Journal of Geophysical Research Atmospheres 109, 117-132.

Chang, C.F., Chen, N.S., Coward, M.P., Deng, W.M., Dewey, J.F., Gansser, A., Harris, N.B.W., Jin, C.W., Kidd, W.S.F., Leeder, M.R., Li, H., Lin, J.L., Liu, C.J., Mei, H.J., Molnar, P., Pan, Y., Pan, Y.S., Pearce, J.A., Shackleton, R.M., Smith, A.B., Sun, Y.Y., Ward, M., Watts, D.R., Xu, J.T., Xu, R.H., Yin, J.X., Zhang, Y.Q., 1986. Preliminary conclusions of the Royal Society and Academia Sinica 1985 geotraverse of Tibet. Nature 323, 501-507.

Chung, S.L., Chu, M.F., Zhang, Y., Xie, Y., Lo, C.H., Lee, T.Y., Lan, C.Y., Li, X., Zhang, Q., Wang, Y., 2005. Tibetan tectonic evolution inferred from spatial and temporal variations in post-collisional magmatism. Earth Science Reviews 68, 173-196.

Clark, M.K., Bush, J.W.M., Royden, L.H., 2005a. Dynamic topography produced by lower crustal flow against rheological strength heterogeneities bordering the Tibetan Plateau. Geophysical Journal International 162, 575-590.

Clark, M.K., House, M.A., Royden, L.H., Whipple, K.X., Burchfiel, B.C., Zhang, X., Tang, W., 2005b. Late Cenozoic uplift of southeastern Tibet. Geology 33, 525-528.

Clift, P.D., 2006. Controls on the erosion of Cenozoic Asia and the flux of clastic sediment to the ocean. Earth and Planetary Science Letters 241, 571-580.

Cook, K.L., Royden, L.H., Burchfiel, B.C., Lee, Y.H., Tan, X., 2013. Constraints on Cenozoic tectonics in the southwestern Longmen Shan from low-temperature thermochronology. Lithosphere 5, 393-406.

Ding, L., Xu, Q., Yue, Y.H., Wang, H.Q., Cai, F.L., Li, S., 2014. The Andean-type Gangdese Mountains: Paleoelevation record from the Paleocene-Eocene Linzhou Basin. Earth and Planetary Science Letters 392, 250-264.

Ehlers, T.A., 2005. Crustal Thermal Processes and the Interpretation of Thermochronometer Data. Reviews in Mineralogy and Geochemistry 58, 315-350.

England, P., Molnar, P., 1990. Surface uplift, uplift of rocks, and exhumation of rocks. Geology 18, 1173.

Enkelmann, E., Ratschbacher, L., Jonckheere, R., Nestler, R., Fleischer, M., Gloaguen, R., Hacker, B.R., Zhang, Y.Q., Ma, Y.S., 2006. Cenozoic exhumation and deformation of northeastern Tibet and the Qinling: Is Tibetan lower crustal flow diverging around the Sichuan Basin? Geological Society of America Bulletin 118, 651-671.

Farley, K., 2000, Helium diffusion from apatite: General behavior as illustrated by Durango fluorapatite: Journal of Geophysical Research-Solid Earth 105, 2903-2914.

Farley, K.A., 2002. (U-Th)/He Dating: Techniques, Calibrations, and Applications. Reviews in Mineralogy and Geochemistry, 47(1): 819-844.

Fielding, E., Isacks, B., Barazangi, M., Duncan, C., 1994. How flat is Tibet? Geology 22, 163-167.

Fitzgerald, P.G., Sandiford, M., Barrett, P.J., Gleadow, A.J.W., 1986. Asymmetric extension associated with uplift and subsidence in the Transantarctic Mountains and Ross Embayment. Earth and Planetary Science Letters, 81(1): 67-78.

Fitzgerald, P.G., Baldwin, S.L., Webb, L.E., O'Sullivan, P.B., 2006. Interpretation of (U-Th)/He single grain ages from slowly cooled crustal terranes: A case study from the Transantarctic Mountains of southern Victoria Land. Chemical Geology, 225(1-2): 91-120.

Flowers, R.M., Ketcham, R.A., Shuster, D.L., Farley, K.A., 2009. Apatite (U-Th)/He thermochronometry using a radiation damage accumulation and annealing model. Geochimica et Cosmochimica Acta 73, 2347-2365.

Fu, P., Harbor, J.M., Stroeven, A.P., Hättestrand, C., Heyman, J., Zhou, L.P., 2013. Glacial geomorphology and paleoglaciation patterns in Shaluli Shan, the southeastern Tibetan Plateau — Evidence for polythermal ice cap glaciation. Geomorphology 182, 66-78.

Galbraith,R. F., 1990. The radial plot: graphical assessment of spread in ages, Nuclear Tracks and Radiation Measurements 17, 207-214.

Gleadow, A.J.W., Kohn, B.P., Brown, R.W., Belton, D.X., 2002. Fission Track Dating of Phosphate Minerals and the Thermochronology of Apatite. Reviews in Mineralogy and Geochemistry 48, 579-630.

Godard, V., Pik, R., Lave, J., Cattin, R., Tibari, B., de Sigoyer, J., Pubellier, M., Zhu, J., 2009. Late Cenozoic evolution of the central Longmen Shan, eastern Tibet: Insight from (U-

Th)/He thermochronometry. Tectonics 28, TC5009.

Guenthner, W.R., Reiners, P.W., Tian, Y.T., 2014. Interpreting date-eU correlations in zircon (U-Th)/He datasets: A case study from the Longmen Shan, China. Earth and Planetary Science Letters 403, 328-339.

Gourbet, L., Mahéo, G., Leloup, P.H., JeanLouis, P., Sorrel, P., Eymard, I., Antoine, P.-O., Sterb, M., Wang, G., Cao, K., Chevalier, M., Lu, H., 2015. The Jianchuan Basin, Yunnan: Implications on the Evolution of SE Tibet During the Eocene, AGU Fall meeting, San Francisco.

Hoke, G.D., Liu-Zeng, J., Hren, M.T., Wissink, G.K., Garzione, C.N., 2014. Stable isotopes reveal high southeast Tibetan Plateau margin since the Paleogene. Earth and Planetary Science Letters 394, 270-278.

House, M.A., Farley, K.A., Stockli, D., 2000. Helium chronometry of apatite and titanite using Nd-YAG laser heating. Earth and Planetary Science Letters 183, 365-368.

Ketcham, R. A., Gautheron, C., Tassan-Got, L., 2011. Accounting for long alpha-particle stopping distances in (U–Th–Sm)/He geochronology: Refinement of the baseline case. Geochimica et cosmochimica acta 75, 7779-7791.

Kirby, E., Reiners, P.W., Krol, M.A., Whipple, K.X., Hodges, K.V., Farley, K.A., Tang, W.Q., Chen, Z.L., 2002. Late Cenozoic evolution of the eastern margin of the Tibetan Plateau: Inferences from $^{40}$Ar/$^{39}$Ar and (U-Th)/He thermochronology. Tectonics 21, 1-20.

Leloup, P.H., Arnaud, N., Lacassin, R., Kienast, J., Harrison, T., Trong, T.T.P., Replumaz, A., Tapponnier, P., 2001. New constraints on the structure, thermochronology, and timing of the Ailao Shan-Red River shear zone, SE Asia. Journal of Geophysical Research 106, 6683-6732.

Li, S.Y., Currie, B.S., Rowley, D.B., Ingalls, M., 2015. Cenozoic paleoaltimetry of the SE margin of the Tibetan Plateau: Constraints on the tectonic evolution of the region. Earth and Planetary Science Letters 432, 415-424.

Liu, J.L., Song, Z.J., Cao, S.Y., Zhai, Y.F., Wang, A.J., Gao, L., Xiu, Q.Y., Cao, D.H., 2006. The dynamic setting and processes of tectonic and magmatic evolution of the oblique collision zone between Indian and Eurasian plates: exemplified by the tectonic evolution of the Three River region, eastern Tibet. Acta Petrologica Sinica 22, 775-786 (in Chinese with English abstract).

Liu, Z., Wang, C., Yi, H., 2001. Evolution and Mass Accumulation of the Cenozoic Hoh Xil Basin, Northern Tibet. Journal of Sedimentary Research 71, 971-984.

Liu-Zeng, J., Tapponnier, J. P., Gaudemer, Y., and Ding, L., 2008, Quantifying landscape differences across the Tibetan plateau: Implications for topographic relief evolution: J. Geophys. Res., 113, F04018, doi:10.1029/2007JF000897.

Lu, Y.J., Campbell McCuaig, T., Li, Z.X., Jourdan, F., Hart, C.J.R., Hou, Z.Q., Tang, S.H., 2015. Paleogene post-collisional lamprophyres in western Yunnan, western Yangtze Craton: Mantle source and tectonic implications. Lithos 233, 139-161.

Lu, Y.J., Kerrich, R., Cawood, P.A., McCuaig, T.C., Hart, C.J., Li, Z.X., Hou, Z.Q., Bagas, L., 2012. Zircon SHRIMP U–Pb geochronology of potassic felsic intrusions in western Yunnan, SW China: Constraints on the relationship of magmatism to the Jinsha suture. Gondwana Research 22, 737-747.

McPhillips, D., Hoke, G.D., Liu-Zeng, J., Bierman, P.R., Rood, D.H., Niedermann, S., 2016. Dating the incision of the Yangtze River Gorge at the First Bend using three-nuclide burial ages. Geophysical Research Letters 43, 101-110.

Meesters, A.G.C.A., Dunai, T.J., 2002. Solving the production-diffusion equation for finite diffusion domains of various shapes: Part I. Implications for low-temperature (U-Th)/He thermochronology. Chemical Geology 186, 333-344.

Molnar, P., Tapponnier, P., 1975. Cenozoic Tectonics of Asia: Effects of a Continental

Collision. Science 189, 419-426.

Ouimet, W., Whipple, K., Royden, L., Reiners, P., Hodges, K., Pringle, M., 2010. Regional incision of the eastern margin of the Tibetan Plateau. Lithosphere 2, 50.

Owen, L.A., 2010. Landscape development of the Himalayan-Tibetan orogen: a review. Geological Society, London, Special Publications 338, 389-407.

Patriat, P., Achache, J., 1984. India-Eurasia collision chronology has implications for crustal shortening and driving mechanism of plates. Nature 311, 615-621.

Powell, C.M., Conaghan, P.J., 1973. Plate tectonics and the Himalayas. Earth and Planetary Science Letters 20, 1-12.

Sato, K., Liu, Y.Y., Wang, Y.B., Yokoyama, M., Yoshioka, S.y., Yang, Z.Y., Otofuji, Y., 2007. Paleomagnetic study of Cretaceous rocks from Pu'er, western Yunnan, China: Evidence of internal deformation of the Indochina block. Earth and Planetary Science Letters 258, 1-15.

SBGMR, 1991. Sichuan Bureau of Geology and Mineral Resources. Regional Geology of Sichuan Province, 728 pp., Geology House, Beijing.

Schoenbohm, L.M., Burchfiel, B.C., Chen, L., 2006. Propagation of surface uplift, lower crustal flow, and Cenozoic tectonics of the southeast margin of the Tibetan Plateau. Geology 34, 813-816.

Shen, Z.K., Lv, J.N., Wang, M., Burgmann, R., 2005. Contemporary crustal deformation around the southeast borderland of the Tibetan Plateau. Journal of Geophysical Research 110, 1-17.

Spiegel, C., Kohn, B., Belton, D., Berner, Z., Gleadow, A., 2009. Apatite (U–Th–Sm)/He thermochronology of rapidly cooled samples: The effect of He implantation. Earth and Planetary Science Letters 285, 105-114.

Spurlin, M.S., Yin, A., Horton, B.K., Zhou, J.Y., Wang, J.H., 2005. Structural evolution of the Yushu-Nangqian region and its relationship to syn-collisional igneous activity, east-central Tibet. Geological Society of America Bulletin 117, 1293-1317.

Tapponnier, P., Xu, Z.Q., Roger, F., Meyer, B., Arnaud, N., Wittlinger, G., J.S., Y., 2001. Oblique Stepwise Rise and Growth of the Tibet Plateau. Science 294, 1671-1677.

Tian, Y.T., Kohn, B.P., Gleadow, A.J., Hu, S.B., 2013. Constructing the Longmen Shan eastern Tibetan Plateau margin: Insights from low-temperature thermochronology. Tectonics 32, 576-592.

Tian, Y.T., Kohn, B.P., Gleadow, A.J.W., Hu, S.B., 2014. A thermochronological perspective on the morphotectonic evolution of the southeastern Tibetan Plateau. Journal of Geophysical Research: Solid Earth 119, 676-698.

Tian, Y.T., Kohn, B.P., Hu, S.B., Gleadow, A.J.W., 2015. Synchronous fluvial response to surface uplift in the eastern Tibetan Plateau: Implications for crustal dynamics. Geophysical Research Letters 42, 29-35.

Wan, S.K., Xia, B., Zhang, Y.Q., 2005. SHRIMP zircon U-Pb dating of Laojunshan syenite. Geotectonica et Metallogenia 29, 522-526 (in Chinese with English abstract).

Wang, C.S., Zhao, X.X., Liu, Z.F., Lippert, P.C., Graham, S.A., Coe, R.S., Yi, H.S., Zhu, L.D., Liu, S., Li, Y.L., 2008. Constraints on early uplift history of the Tibetan Plateau. Proceedings of the National Academy of Sciences 105, 4987-4992.

Wang, E., Burchfiel, B.C., 1998. Late Cenozoic Xianshuihe-Xiaojiang, Red River, and Dali fault systems of southwestern Sichuan and central Yunnan, China. Geological Society of America Special Paper 327, 1-108.

Wang, E., Kirby, E., Furlong, K., van Soest, M., Xu, G., Shi, X., Kamp, P., Hodges, K., 2012. Two-phase growth of high topography in eastern Tibet during the Cenozoic. Nature Geoscience 5, 640-645.

Wang, J.H., Yin, A., Harrison, T.M., Grove, M., Zhang, Y.Q., Xie, G.H., 2001. A tectonic model for Cenozoic igneous activities in the eastern Indo–Asian collision zone. Earth and Planetary Science Letters 188, 123-133.

Wang, Y.J., Fan, W.M., Zhang, Y.H., Peng, T.P., Chen, X.Y., Xu, Y.G., 2006. Kinematics and $^{40}Ar/^{39}Ar$ geochronology of the Gaoligong and Chongshan shear systems, western Yunnan, China: Implications for early Oligocene tectonic extrusion of SE Asia. Tectonophysics 418, 235-254.

Yang, J.Q., Zhang, W., Cui, Z.J., Yi, C.L., Liu, K.X., Ju, Y.j., Zhang, X.Y., 2006. Late Pleistocene glaciation of the Diancang and Gongwang Mountains, southeast margin of the Tibetan plateau. Quaternary International 154–155, 52-62.

Yang, R., Willett, S. D., and Goren, L., 2015, In situ low-relief landscape formation as a result of river network disruption: Nature 520, 526-529.

Yang, R., Fellin, M.G., Herman, F., Willett, S.D., Wang, W., Maden, C., 2016. Spatial and temporal pattern of erosion in the Three Rivers Region, southeastern Tibet. Earth Planet. Sci. Lett. 433, 10-20.

Yang, T.N., Liang, M.J., Fan, J.W., Shi, P.L., Zhang, H.R., Hou, Z.H., 2014. Paleogene sedimentation, volcanism, and deformation in eastern Tibet: Evidence from structures, geochemistry, and zircon U-Pb dating in the Jianchuan Basin, SW China. Gondwana Research 26, 521-535.

YBGMR, 1974. Yunnan Bureau of Geology and Mineral Resource (YBGMR). Geological map (scale 1/200,000) with geological report of Lanping (block G-47-X VI).

YBGMR, 1984. Yunnan Bureau of Geology and Mineral Resource (YBGMR). Geological map (scale 1/200,000) with geological report of Weixi (block G-47-X).

Yin, A., Harrison, T.M., 2000. Geologic Evolution of the Himalayan-Tibetan Orogen. Annual Review of Earth and Planetary Sciences 28, 211-280.

Zachos, J.C., Dickens, G.R., Zeebe, R.E., 2008. An early Cenozoic perspective on greenhouse warming and carbon-cycle dynamics. Nature 451, 279-283.

Zhao, G.G., 1965. Preliminary observations on the structure and Cenozoic deposition in the Lijiang-Dali region of western Yunnan. Geological Review 23, 346-355.

Zheng, H.B., Clift, P.D., Wang, P., Tada, R., Jia, J.T., He, M.Y., Jourdan, F., 2013. Pre-Miocene birth of the Yangtze River. Proceedings of the National Academy of Sciences 110, 7556-7561.

**Figure Captions:**

Figure 1. Tectonics and regional topography of the eastern Tibetan Plateau. Inserted panel: neotectonic framework of the Tibetan Plateau, showing location of the study area (shaded rectangle). Abbreviations: ATF = Altyn Tagh Fault; GXF = Ganze-Xianshuihe Fault; HF = Haiyuan Fault; JF = Jiali Fault; KLF = Kunlun Fault; RRF = Red River Fault; SB = Sichuan Basin; SF = Sagaing fault; TB = Tarim Basin; TP = Tibetan Plateau. Also shown are previous determinations for the age of onset of river incision at sites marked by grey stars. Reference codes are: 1 = Clark et al., (2005b); 2 = Ouimet et al., (2010); 3 = Wang et al., (2012); 4 = Kirby et al., (2002) and Wang et al., (2012); 5 = Tian et al., (2013), Cook et al., (2013), and Guenthner et al., (2014); 6 = Tian et al. (2014); 7 = Tian et al. (2015); 8 = Hoke et al. (2014); 9 = Li et al. (2015); 10 = McPhillips et al. (2016). The star filled in white shows the locality of this study.

Figure 2. Topographic map (SRTM) of the study area, showing the samples locations, river network and Cenozoic faults. The samples were collected from a tributary nearby the first bend of the Yangtze River.

Figure 3. Generalized geological map of the study area, modified after YBGMR, (1984). Also compiled are sample localities and previously reported SHRIMP U-Pb results by Lu et al. (2012).

Figure 4. Plots of AHe ages versus effective uranium concentration [eU] (a), and equivalent radius (Rs), the radius of a sphere with an equivalent surface area-to-volume ratio as the cylindrical crystals (b).

Figure 5. Plot of AHe age versus elevation. Excluding the six abnormally old ages plotted in grey, the age-elevation relationship yields an erosion rate of ~0.10-0.18 m/yr. The cyan regions marks the range of zircon U/Pb ages.

**Tables:**

Table 1. Information of samples reported in this study

Table 2. Results of single-grain apatite (U-Th-Sm)/He dating

**Appendix A1**

For AFT analysis, grains were mounted in epoxy resin on glass slides, ground and polished to an optical finish to expose internal grain surfaces. Mounts were etched in 5M $HNO_3$ for 20 seconds at 21°C to reveal the fossil tracks and possible dislocations in the crystal structure. Apatite grains of all samples from the Laojunshan intrusion are found to be rich in dislocations, which are often curved and parallel after being etched. Apatite of this kind is not suitable for fission-track dating, because some dislocations may be too similar to fission-tracks to be identified.

Figure A1: (a) A representative photo of etched apatite fission-track mount from the Laojunshan intrusion (SG1407), showing the presence of numerous crystal dislocations, which are often curved and parallel after being etched. (b-c) Close-up views of curved and parallel dislocations in panel (a).

**Figures and captions:**

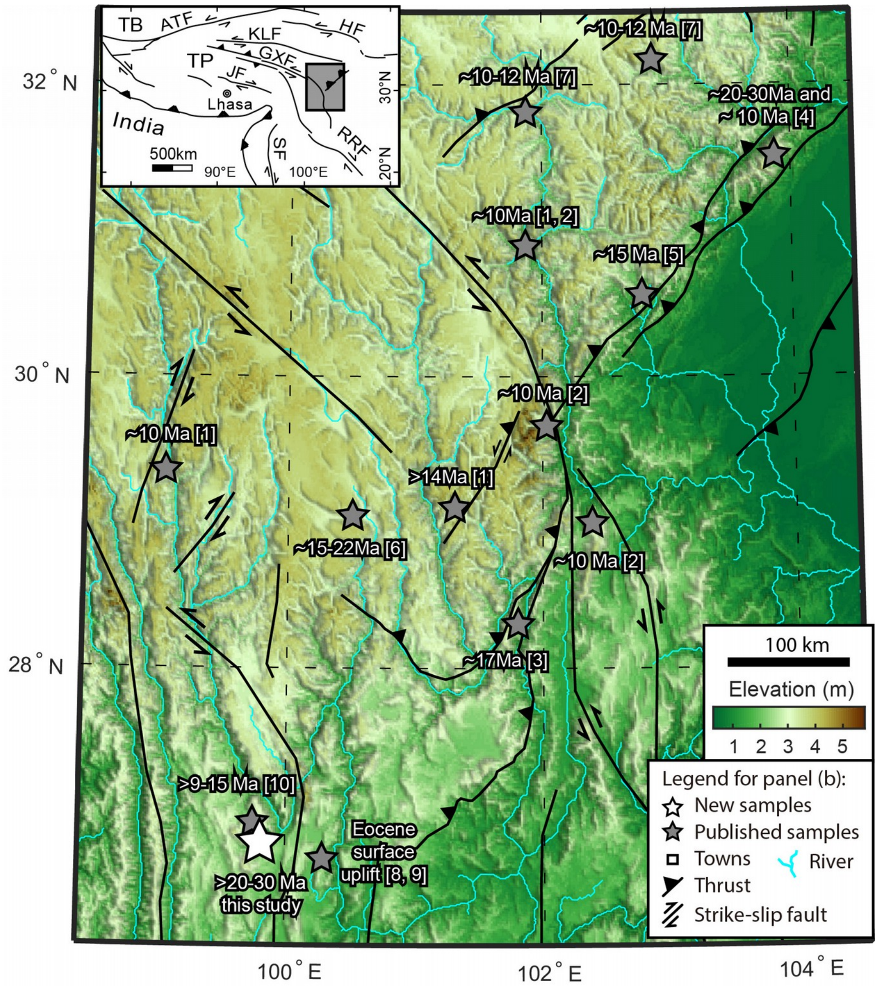


Figure 1. Tectonics and regional topography of the eastern Tibetan Plateau. Inserted panel: neotectonic framework of the Tibetan Plateau, showing location of the study area (shaded rectangle). Abbreviations: ATF = Altyn Tagh Fault; GXF = Ganze-Xianshuihe Fault; HF = Haiyuan Fault; JF = Jiali Fault; KLF = Kunlun Fault; RRF = Red River Fault; SB = Sichuan Basin; SF = Sagaing fault; TB = Tarim Basin; TP = Tibetan Plateau. Also shown are previous determinations for the age of onset of river incision at sites marked by grey stars. Reference codes are: 1 = Clark et al., (2005b); 2 = Ouimet et al., (2010); 3 = Wang et al., (2012); 4 = Kirby et al., (2002) and Wang et al., (2012); 5 = Tian et al., (2013), Cook et al., (2013), and Guenthner et al., (2014); 6 = Tian et al. (2014); 7 = Tian et al. (2015); 8 = Hoke et al. (2014); 9 = Li et al. (2015); 10 = McPhillips et al. (2016). The star filled in white shows the locality of this study.

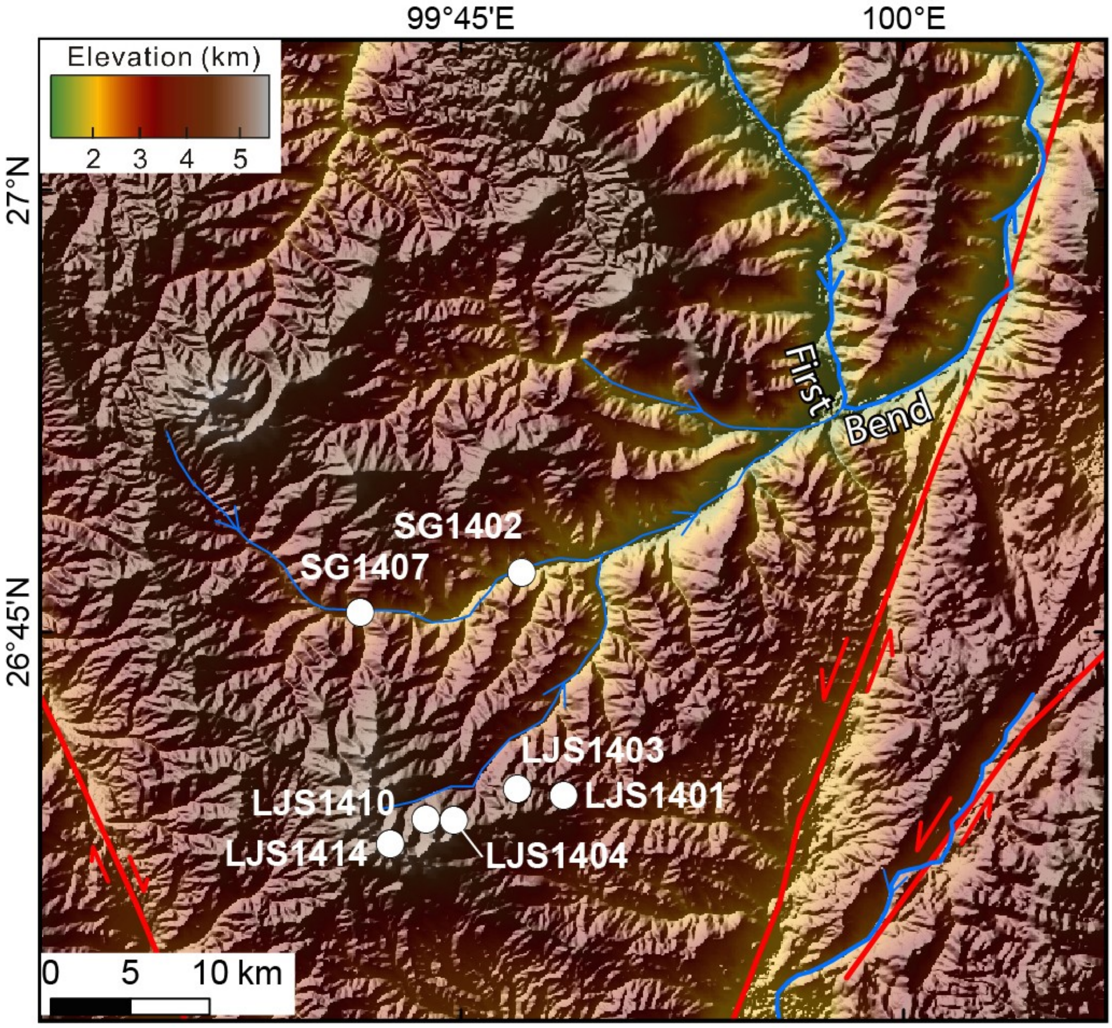


Figure 2. Topographic map (SRTM) of the study area, showing the samples locations, river network and Cenozoic faults. The samples were collected from a tributary nearby the first bend of the Yangtze River.

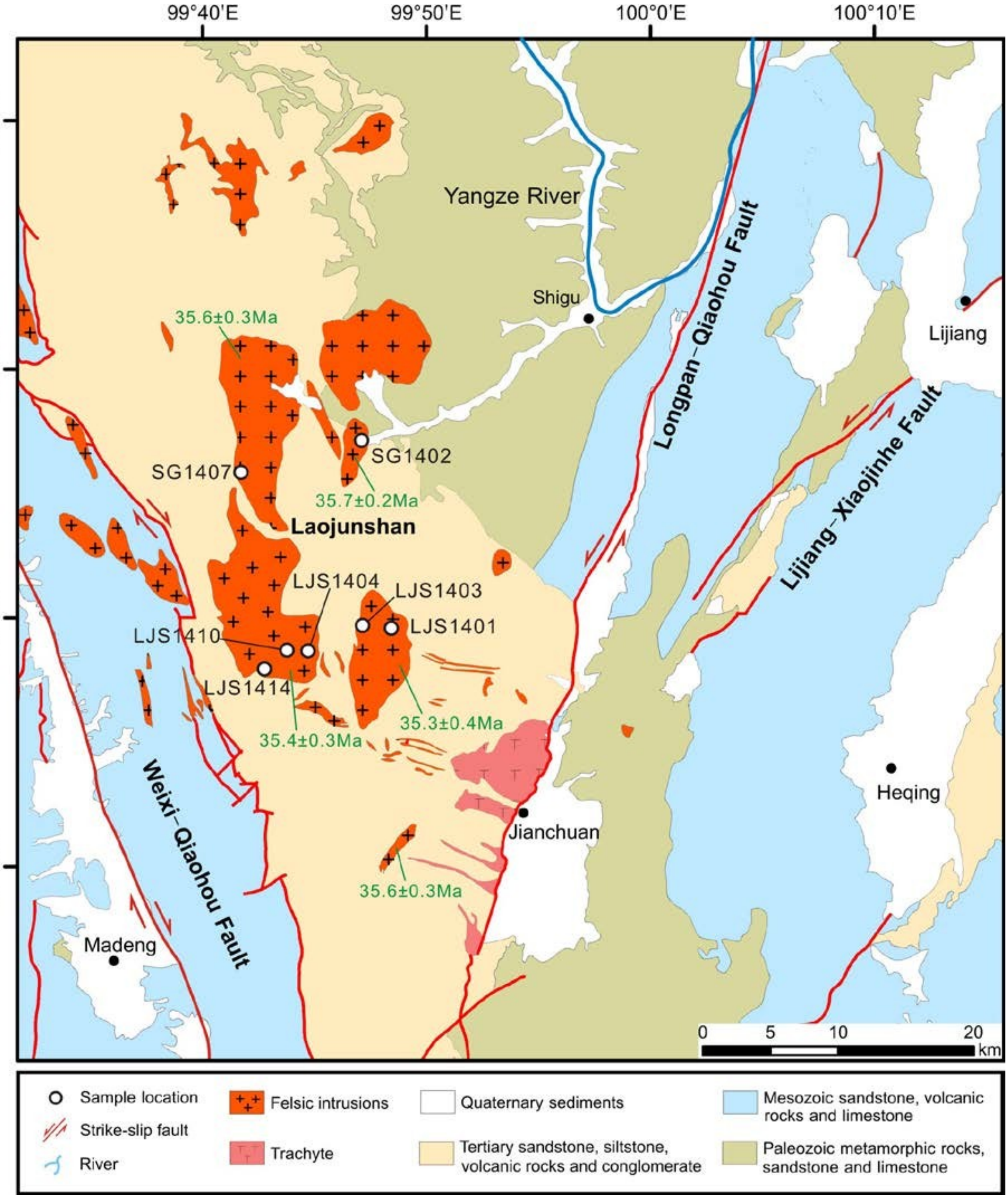


Figure 3. Generalized geological map of the study area, modified after YBGMR, (1984). Also compiled are sample localities and previously reported SHRIMP U-Pb results by Lu et al. (2012).

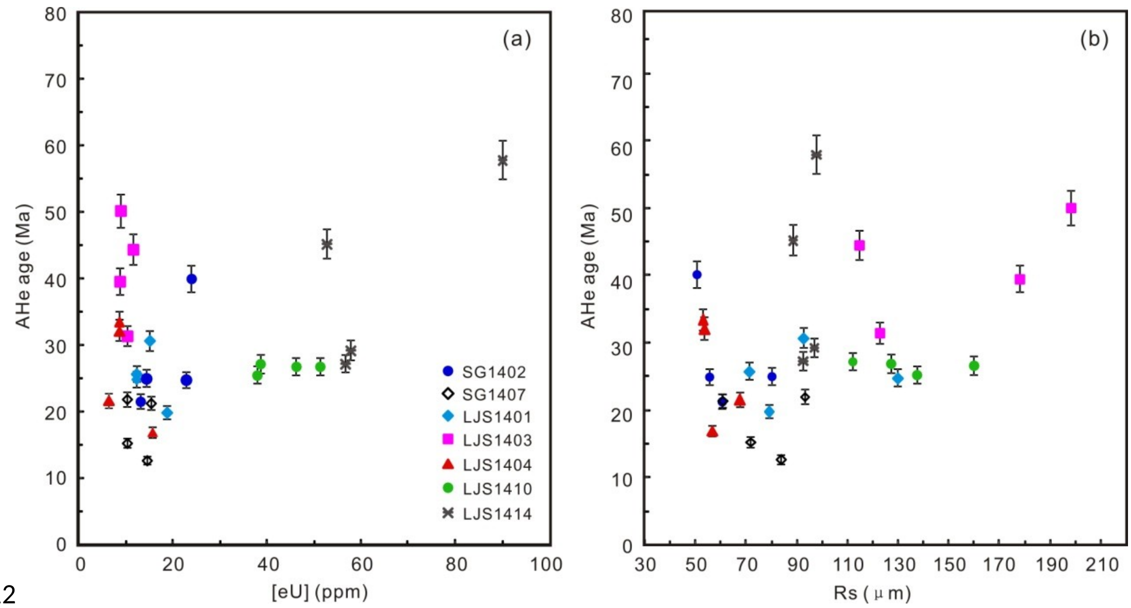


Figure 4. Plots of AHe ages versus effective uranium concentration [eU] (a), and equivalent radius (Rs), the radius of a sphere with an equivalent surface area-to-volume ratio as the cylindrical crystals (b).

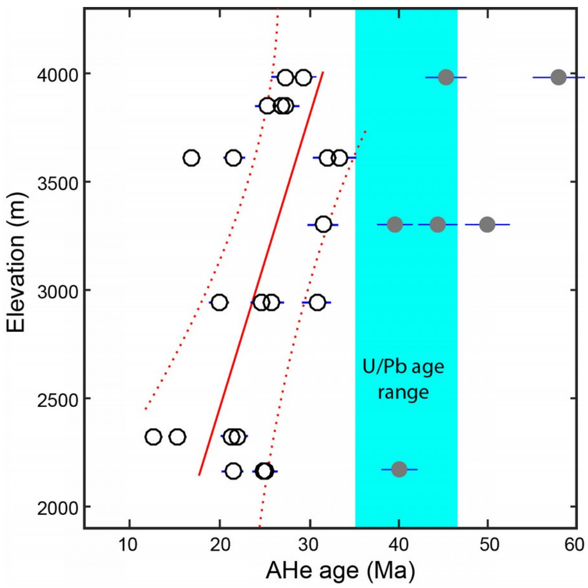


Figure 5. Plot of AHe age versus elevation. Excluding the six abnormally old ages plotted in grey, the age-elevation relationship yields an erosion rate of ~0.10-0.18 m/yr. The cyan regions marks the range of zircon U/Pb ages.

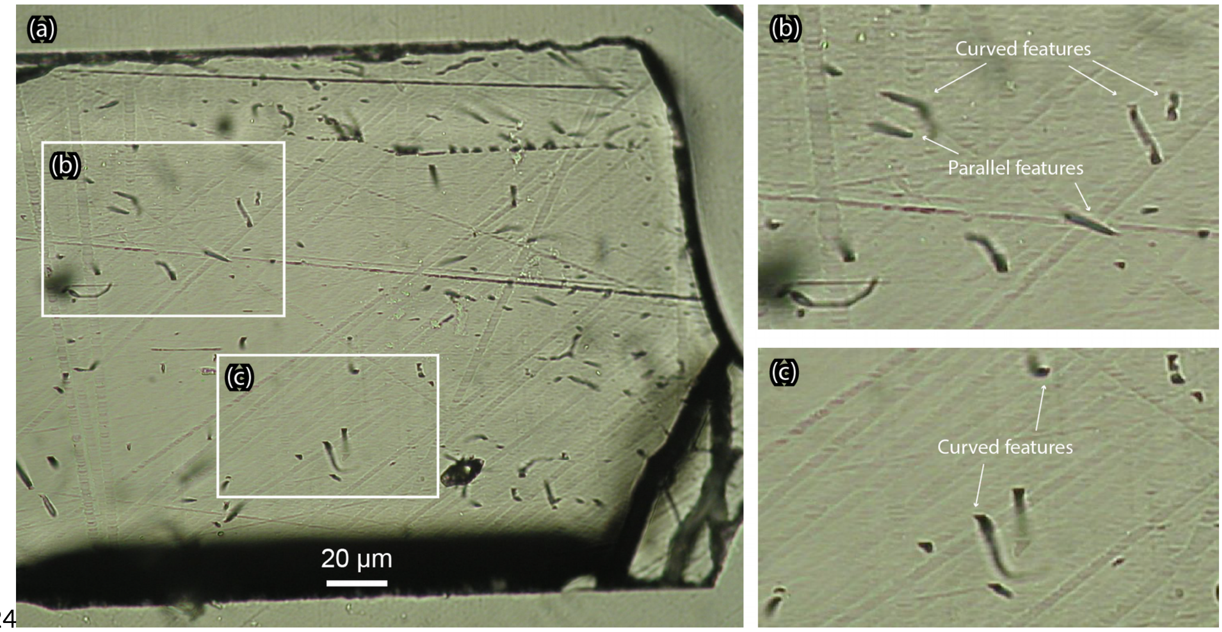


Figure A1: (a) A representative photo of etched apatite fission-track mount from the Laojunshan intrusion (SG1407), showing the presence of numerous crystal dislocations, which are often curved and parallel after being etched. (b-c) Close-up views of curved and parallel dislocations in panel (a).